J. Fluid Mech. (2005), *vol.* 525, *pp.* 27–36.
DOI: 10.1017/S0022112004002642 Printed in the United Kingdom

Flow between rotating finite disks with a closed end condition studied by heterodyne photon-correlation

By R. DI LEONARDO, F. IANNI AND G. RUOCCO

Department of Physics, University of Rome La Sapienza, P.le Aldo Moro 2, 00185, Italy

(Received 31 July 2004 and in revised form 8 November 2004)

We have investigated experimentally the swirling flow between a stationary and a rotating disk with fixed closed end. In order to perform velocimetry measurements we implemented a heterodyne photon-correlation setup and obtained the three components of the velocity field at different positions along the gap between the disks. We compared the results for two different Reynolds numbers with a numerical solution of the similarity equation, to investigate the relation between the finite and infinite disk solution, theoretically studied by Brady & Durlofsky (1987). For the measurements performed at Re below the critical Reynolds number $Re_C = 80$, we found that the two solutions agree very well near the axis of rotation. Above Re_C we found that this quantitative agreement no longer holds, but the flow qualitatively resembles the Batchelor solution, with two boundary layers and a core rotating as a solid body. Our results validate the theoretical prediction for closed-end finite disk flow.

1. Introduction

The flow driven by parallel rotating disks, often called swirling flow, has been a topic of great interest for many decades. It has technical applications in several different fields, such as viscometry, lubrication, rotating machinery, geophysics, crystal growth processes. From a theoretical point of view, this interest is due to the existence – for the flow driven by rotating disks of infinite extent in an unbounded fluid – of an exact representation of the Navier–Stokes equations as a system of ordinary differential equations. Thus, measurements of the velocity field of the flow are of interest to validate this theoretical solution.

The first work on the rotating disk flows is that of von Kármán (1921), who theoretically studied an incompressible flow over an infinite rotating disk in a fluid that is stationary far from the disk. By assuming a self-similar, axisymmetric velocity profile, he found that the Navier–Stokes equations could be reduced exactly to a set of nonlinear ordinary differential equations, called similarity equations. Numerical solution of this system shows that the disk pulls the fluid radially outward in a region above the disk and draws it in axially, as one would intuitively expect from centrifugal effects and continuity in the flow. Batchelor (1951) and Stewartson (1953) extended the study of von Kármán to the case of two infinite, coaxial rotating disks a distance H apart. For this geometry the von Kármán similarity principle still applies and a Reynolds number (Re) based on H – the only characteristic length of the problem – is introduced. In the case of one fixed and one rotating disk, they found different solutions to the problem: Batchelor, based on qualitative arguments, predicted a flow

with two separated boundary layers close to the disks and a core rotating as a solid body; while Stewartson found only one boundary layer on the rotating disk and a non-rotating core. In fact, their solutions are two of several solutions that appear as the Reynolds number is increased: Zandbergen & Dijkstra (1987) showed that non-unique solution structures appear as Re increases above ~ 55. So the Batchelor solution is valid at low Reynolds number, while Stewartson's exists for Reynolds numbers over 200.

The case where the radius of the disks is finite is of practical importance and experimental verification of the similarity solution can only be obtained with finite disks. So the question of whether and to what extent the similarity solution occurs in a finite radial geometry is of interest. Brady & Durlofsky (1987) studied numerically the flow between finite but large disks, distinguishing between a closed and an open end condition. They showed that the finite disk and the similarity solutions generally coincide over smaller and smaller portions of the flow domain with increasing Reynolds number, for both end conditions.

In this work we use the heterodyne light beating spectroscopy technique (Cummins & Swinney 1970; Drain 1980) which was developed in the 1960s: here we improve the technique by implementing a novel setup (Salmon *et al.* 2003) which uses an optical fibre collecting device, ensuring a better optical matching of the two interfering beams. Through this technique, we determine the vectorial velocity field of a Newtonian fluid (water–glycerol mixture) in a swirling flow. More specifically, we study the stationary, non-trivial flow between a rotating and a fixed disk with closed end condition as a function of the position along the gap. Bien & Penner (1969) have already studied the swirling flow under these conditions and, using the heterodyne light beating spectroscopy technique, measured the azimuthal velocity component. Dijkstra & van Heijst (1982), using a stereophotography technique, measured the azimuthal and radial components of the velocity field: they found that the fluid far from the disk end follows the Batchelor solution for infinite disks. In our work we have measured all three velocity field components: these data, for the flow between two rotating disks (having a radius much bigger than the spacing between them), were previously unavailable in the literature (Prasad & Adrian 1992). Our aim is to experimentally show the validity of Brady & Durlofsky's solution for closed end conditions and small Reynolds number. The heterodyne photon-correlation technique we implemented can also be used to investigate complex fluids under shear (Larson 1998), which show non-Newtonian behaviour such as shear thinning, shear banding and wall slip: these phenomena can be detected through local measurements of the velocity field (Salmon *et al.* 2003).

2. Problem formulation

We denote the radius of the disks by L, the spacing between them by H, the angular velocity of the rotating disk by Ω, the fluid viscosity by η and its density by ρ; the Reynolds number is $Re = \rho \Omega H^2/\eta$. We will use a cylindrical coordinate system (r, φ, z) with the z-axis coinciding with the axis of rotation.

For disks of infinite radius ($L/H \to \infty$), according to the von Kármán similarity principle, the Navier–Stokes equations admit an exact solution of the form

$$\left.\begin{aligned} v_r(r, z) &= -\tfrac{1}{2} r f'(z), \\ v_z(z) &= f(z), \\ v_\varphi(r, z) &= r g(z), \end{aligned}\right\} \tag{2.1}$$

where v_r, v_z, v_φ are the radial, axial and azimuthal components of the velocity field. The similarity functions f and g satisfy a system of two ordinary differential equations (reported in Brady & Durlofsky 1987) with no-slip boundary conditions at both disks, which can be solved numerically.

For the flow between finite but large disks Brady & Durlofsky have written the equations of motion and continuity (obtained with scaling arguments), the no-slip boundary condition in z and the correct boundary conditions in r for the two different end conditions (closed and open). Solving the system numerically, they found that near the outer edge the effect of the end will be important and the flow will not be of the similarity form; in particular, the closed end affects the flow much more than an open end, where the flux lines leave the disk region. As the axis of rotation is approached, however, the effect of the end will decrease and the solution may approach the similarity form. The end effect also depends on Re: on increasing Re the end effect becomes more important and the region where the solutions are alike gets smaller. Thus it is of interest to find for which Reynolds number, at a given radial position, the finite-disk solution resemble the similarity solution. For example, for $Re = 40$, they found that the finite-disk solution agrees with the Batchelor solution (meaning that the two solutions differ by less than 2%) in a region extending to $r = 0.35L$ for an open end, and to $r = 0.2L$ for a closed end. For $Re = 60$ both the open- and closed-end flows still agree with the Batchelor solution up to about $r = 0.1L$, while at the critical value $Re_C = 80$ the two solution agree only in the limit $r \to 0$. At $Re > Re_C$ the effect of the end propagates all the way to the axis of rotation and there is no longer agreement with any similarity solution for both end conditions. However, even for $Re > Re_C$, there is a qualitative resemblance to the similarity solution which is determined by the type of end condition: the open-end flow tends away from the Batchelor solution and toward the Stewartson one, while the closed-end flow continue to resemble the Batchelor solution, with a definite core rotation, up to much higher Re.

In this work we measured the velocity field along the gap, at a given radial distance (in the vicinity of the axis), for two different Reynolds number: one greater than Re_C and one less. By comparing our results with the corresponding numerical solution for infinite disks, we show that Brady & Durlofsky's predictions hold.

3. Experimental set-up

The experimental technique we implemented to measure the velocity field in the swirling flow is the heterodyne photon-correlation, which enabled us to measure all three components of the velocity field. Heterodyne photon-correlation is a dynamic light scattering experiment (Berne & Pecora 1976): a monocromatic wave of visible radiation is emitted by a laser and impinges on the sample; the scattered light of intensity I_s is made interfere with part of the unscattered radiation (representing a local oscillator) of intensity I_{LO}, on the sensitive element of a photomultiplier; finally a correlator calculates the time-correlation function of the intensity of the radiation hitting the photocatode:

$$\langle i(0)i(t)\rangle \sim \langle |E_{LO}(0) + E_s(0)|^2 |E_{LO}(t) + E_s(t)|^2 \rangle$$

where E is the electric field of the radiation of intensity I. Choosing the experimental condition $I_{LO} \gg I_s$, it is easy to show (Cummins & Swinney 1970) that the correlation function reduces to

$$\langle i(0)i(t)\rangle \sim I_{LO}^2 + 2I_{LO} Re[\langle E_s^*(t) E_s(0)\rangle].$$

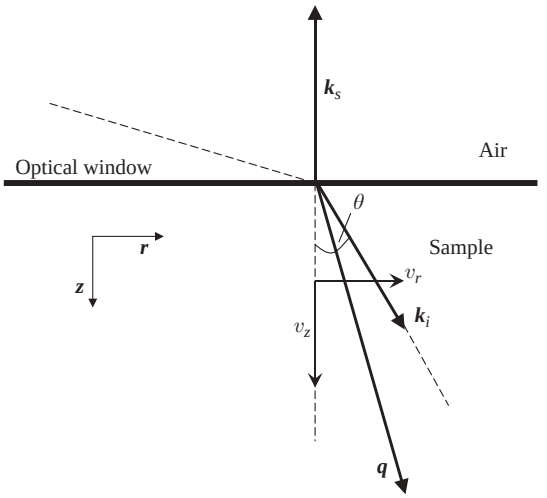

FIGURE 1. Scattering geometry: $\boldsymbol{k}_i$ is the incident wave vector, $\boldsymbol{k}_s$ the scattered one, $\boldsymbol{q}$ the exchanged wave vector, v_r is the radial component and v_z the axial component of the velocity field.

For randomly distributed particles and neglecting the transit time effect, we can write

$$\langle E_s^*(t)E_s(0)\rangle = \left\langle \sum_j W(r_j)\mathrm{e}^{\mathrm{i}\boldsymbol{q}\cdot[\boldsymbol{r}_j(t)-\boldsymbol{r}_j(0)]} \right\rangle \tag{3.1}$$

where $W(\boldsymbol{r})$ represents the scattering volume profile (Ricka 1993). In a sufficiently viscous fluid and for short time scales, particles will move with the fluid velocity field $\boldsymbol{v}$ and with negligible Brownian displacement: denoting as $\boldsymbol{v}_0$ the fluid velocity field in the centre of the scattering volume, where we take the origin for the spatial coordinate $\boldsymbol{r}$, we can write

$$\boldsymbol{r}_j(t) - \boldsymbol{r}_j(0) = \boldsymbol{v}_0 t + \nabla\omega\cdot\boldsymbol{r}t \tag{3.2}$$

with $\omega = \boldsymbol{q}\cdot\boldsymbol{v}$, $\boldsymbol{q}$ being the scattering vector: $\boldsymbol{q} = \boldsymbol{k}_i - \boldsymbol{k}_s$, where $\boldsymbol{k}_i$ and $\boldsymbol{k}_s$ are the wave vectors, respectively, of the incident and scattered beams. (See figure 1.) Substituting (3.2) in (3.1) gives

$$Re[\langle E_s^*(t)E_s(0)\rangle] \propto \widetilde{W}(\nabla\omega t)\cos(\boldsymbol{q}\cdot\boldsymbol{v}_0 t) \tag{3.3}$$

where $\widetilde{W}$ is the spatial Fourier transform of W and therefore vanishes when $t \gtrsim 1/L|\nabla\omega|$ with L the scattering volume size. It is easy to realize that, on the time scale set by the decay of $\widetilde{W}$, our assumption of a negligible Brownian displacement is verified.

Thus, knowing the $\boldsymbol{q}$ vector, we can calculate the projection of the velocity field $\boldsymbol{v}_0$ over $\boldsymbol{q}$ from the period of the measured, oscillating correlation function. The fact that, due to the presence of the shear, there is a velocity difference in the flow inside the scattering volume (Fuller *et al.* 1980; Tong, Goldburg & Chan 1988) results in the modulation of the oscillation by the decaying function $\widetilde{W}(\nabla\omega t)$.

The cell we used (figure 2) is made up of an optical window, which represents the stationary plate, and a disk of radius $L = 5\,\mathrm{cm}$, which is made rotate at an angular velocity ranging from 1 Hz to 100 Hz by a DC electrical motor with a permanent magnet. The rotating disk is made of glass to avoid uncorrelated noise due to the reflection of the incident beam on the disk surface. The rotational axis is in the horizontal direction and the distance between the disks is $H = 1.45\,\mathrm{cm}$. To allow the disk to rotate,

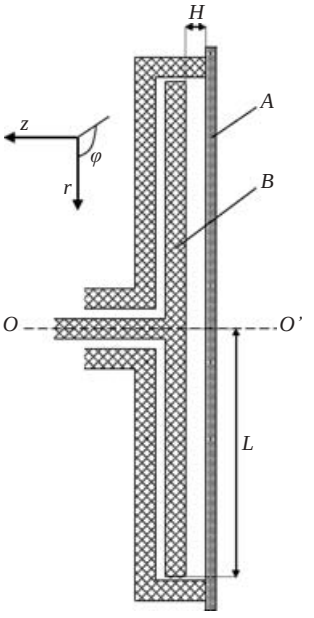

FIGURE 2. Schematic illustration of the cell used in the experiment. It has cylindrical symmetry around the OO'-axis. The fixed disk (A) is a $BK7$ optical window, the rotating disk (B) is made out of glass with a black layer behind to minimize stray light. The body of the cell is made of brass coated by a thin chromium film.

the distance between the glass disk rim and the external wall of the cell is $3\,\text{mm} \ll H$, thus we can approximate the end of the disks as closed.

The Newtonian sample we used is a suspension of latex spheres (made of polystyrene) of diameter 1.05 μm in a solution of glycerol and water: the latex particles, having a large polarizability mismatch, will be responsible for almost all the light scattered by the scattering volume (defined by the intersection between the incident and the scattered beam) and their dynamics will be investigated. In the set-up we used (figure 3), an He – Ne polarized laser beam (35 mW, $\lambda = 633$ nm) is directed, through an optical fibre followed by a collimator (C), towards a beam splitter (BS); one of the two beams coming from BS is directed, through a mirror (M) towards the cell containing the sample (S); the other beam, representing the local oscillator, is attenuated by a filter (A) and collected by a fibre collimator (of focal length 50 mm) followed by a single-mode optical fibre (f_1, core diameter 3.5 μm, OZ Optics). The beam scattered by the sample is collected, in the direction perpendicular to the disks, by another collimator (of focal length 35 mm) and fibre (f_2) couple. Both the fibres are polarization-maintaining and the interference between the scattered field and the local oscillator is achieved through a fibre optics beam splitter ($FOBS$), which matches the wavefronts of the two beams. Another optical fibre (f_3) propagates the interference beam from the beam splitter to the photomultiplier, ensuring spatial coherence of the beam on the photocatode surface. Finally, the digital signal output from the photomultiplier is sent to a correlator designed by the first author Di Leonardo in 2002.

To obtain a direct visualization of the scattering volume we attached the fibre f_1 to the $FOBS$ in place of f_3: the scattering volume is the intersection of the incident beam and the beam coming from f_2. We measure only an average velocity in the scattering volume and the resolution will be given by the scattering volume size: 2 mm

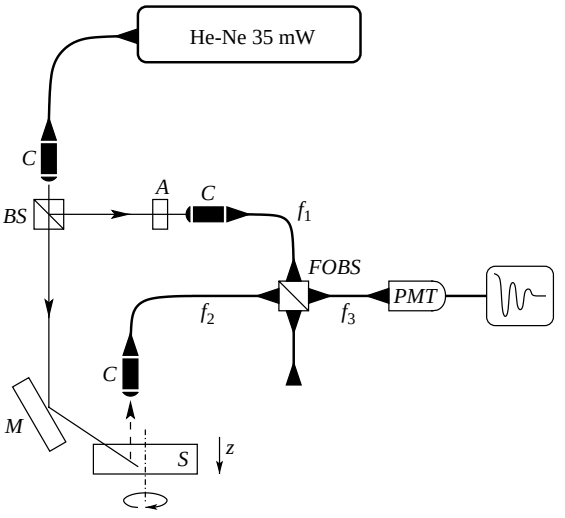

FIGURE 3. Heterodyne set-up. *C*: collimator, *BS*: beam splitter, *A*: filter, *M*: mirror, *S*: sample, *FOBS*: fibre optics beam splitter, *f*: fibre and *PMT*: photomultiplier.

in the z-direction and 3 mm along the radial and y-directions, which is small enough if compared to the gap width $H = 1.42$ cm.

4. Results

We will now present our experimental measurements of the three velocity field components along the gap for the different Reynolds numbers: above and below Re_C. As explained before, the measured correlation function shows oscillations at a frequency corresponding to the velocity field projection over the scattering vector $\boldsymbol{q}$ in the scattering volume. On making a scan along the z-direction, from one disk to the other, the measured correlation functions have the form shown in figure 4 (open circles). Through a micrometer movement of the cell, the scattering volume is moved along the gap in steps of $\Delta z/H = 0.053$, starting from the window and going towards the disk: on the right-hand part of the figure we show the data collected on the window side, on the left-hand part those on the disk side. An exponential decay provides a good fit for the function $\widetilde{W}$ of equation (3.3), so we obtain the frequency ω of the oscillation by fitting the measured signal with an exponential decay function modulated by a cosine: $y = A + B\exp(-t/\tau)\cos\omega t$, which is plotted as a solid line for each measured correlation function.

We performed the scan along z in three different scattering geometries, in order to obtain the three components of the velocity vector for each position of the scattering volume along z. First, we fixed the Reynolds number at $Re_1 = 7.40$ by choosing the angular velocity of the disk of $\Omega = 4.22$ Hz and using a sample of latex spheres in a solution of water in glycerol at a percentage of 13%. The dynamic viscosity was measured by means of homodyne photon-correlation and using the Stokes–Einstein formula; the corresponding kinematic viscosity is $\nu = \eta/\rho = 1.14 \times 10^{-4}\,\mathrm{m^2\,s^{-1}}$. We first fixed the scattering volume at the position $r = 1.0$ cm and $\varphi = \pi/2$ (see figure 2, taking the centre of the fixed disk as the origin of the axis); thus the oscillation frequency can be identified with the sum

$$\omega_1 = v_z|\boldsymbol{q}|\cos\tfrac{1}{2}\theta + v_r|\boldsymbol{q}|\sin\tfrac{1}{2}\theta \tag{4.1}$$

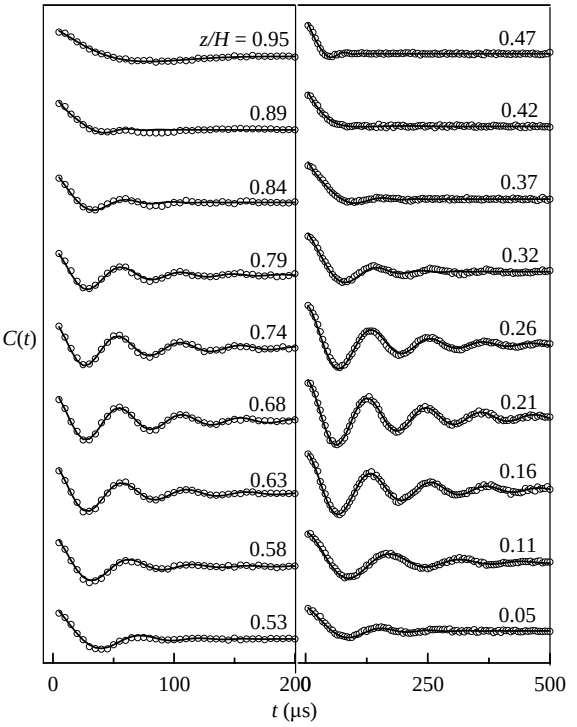

FIGURE 4. Measured correlation functions at fixed radial distance ($r = 1.0\,\text{cm}$) for different positions of the scattering volume along the gap. Each translation is $\Delta z/H = 0.053$ and each correlation function is labelled by the distance of the scattering volume from the optical window in units of z/H. The fitting curve is an exponential modulated cosine. The spectra shown are for $Re = Re_1$ in the second geometry (the one providing equation (4.2)).

where θ is the angle between the incident beam direction and the scattered beam direction (figure 1). The second geometry is like the previous one, apart from the sign of the angle θ, which is the opposite:

$$\omega_2 = v_z|\boldsymbol{q}| \cos \tfrac{1}{2}\theta - v_r|\boldsymbol{q}| \sin \tfrac{1}{2}\theta. \tag{4.2}$$

As we are dealing with low Reynolds number, we can assume that the flow is axisymmetric (Hewitt & Duck 1999). So thirdly we kept the last scattering geometry, but moved the cell vertically and horizontally to bring the scattering volume to the vertical distance $r = 1.0\,\text{cm}$ from the rotational axis ($\varphi = 0$), so that the azimuthal component of the velocity takes the place of the radial one:

$$\omega_3 = v_z|\boldsymbol{q}| \cos \tfrac{1}{2}\theta - v_\varphi|\boldsymbol{q}| \sin \tfrac{1}{2}\theta. \tag{4.3}$$

We calculated the scattering vector $|\boldsymbol{q}| = 4\pi n/\lambda \sin\theta_s/2$ by measuring the scattering angle θ_s and using the known refractive index ($n = 1.45$) of the sample and the wavelength λ of the incident beam. Thus, knowing $\boldsymbol{q}$, it is straightforward to obtain the components v_r, v_z and v_φ of the velocity field as a function of z by solving the system of equations (4.1), (4.2), (4.3) for each position of the scattering volume along the gap. The results are shown in figure 5, where the velocity components are plotted in non-dimensional units $v/\Omega r$. The radial component changes sign at $z = H/2$, in the centre of the gap: by the centrifugal effect the flow is pulled radially outward in the region near the rotating disk and is pushed inward at the other side, near the fixed disk. The

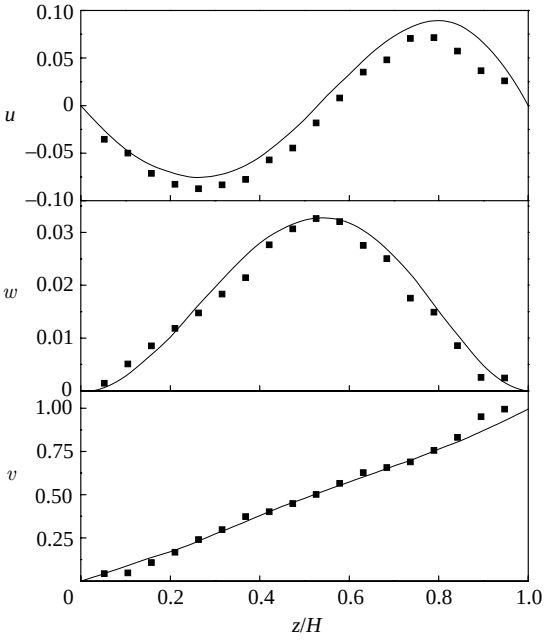

FIGURE 5. Measured velocity profile of the non-dimensional components $u = v_r/\Omega r$, $w = v_z/\Omega r$ and $v = v_\varphi/\Omega r$ at $r = 1.0\,\mathrm{cm}$ for $Re_1 = 7.40$. The lines are the corresponding components for infinite disks extrapolated from Joseph's numerical solution. The error bars are of the same order as the symbols' dimension.

axial component, which is maximum at $z = H/2$, shows that the flow is drawn axially towards the rotating disk, ensuring continuity in the flow. Finally, the azimuthal component is linear from one disk to the other, as was observed at low Reynolds number by Bien & Penner (1969). We observe that, at the boundaries, the velocity components (apart from the azimuthal one on the rotating disk which is expected to be non-zero) do not go to zero as they should: this is an effect of the scattering volume finite size, which could be reduced by focusing the incident and scattered beams. We repeated the same procedure for a higher Reynolds number, increasing the concentration of water in the sample in order to obtain a lower viscosity, also measured by homodyne photon-correlation. The corresponding kinematic viscosity was $\nu = 10.3 \times 10^{-6}\,\mathrm{m^2\,s^{-1}}$; the angular velocity of the disk was fixed at $\Omega = 5.32\,\mathrm{Hz}$, so we obtained a Reynolds number $Re_2 = 104$. Also in this case, we maintained a fixed radial distance of $R = 1.0\,\mathrm{cm}$ for the three scattering geometries. The results for the velocity field components are plotted in figure 6. For this higher Reynolds number, the radial and axial components do not show the symmetry with respect to $z = H/2$, existing at Re_1, and the azimuthal component is no longer linear.

To compare the flow for finite disks with that for infinite disks at the small Reynolds number Re_1, we have plotted the corresponding velocity field components for infinite disks on top of our experimental results. To this end, we interpolate the numerical solution found by Joseph (1990) for the functions f and g of the similarity equations (2.1): the three velocity components so obtained are plotted as a solid line in figure 5. For $Re < Re_C$ we expect, from Brady & Durlofsky's study, that the flow for finite disks is of the similarity form in the region near the axis. In particular, recalling the results reported at the end of § 2, at $Re = 7.4$ we expect that this region extends far

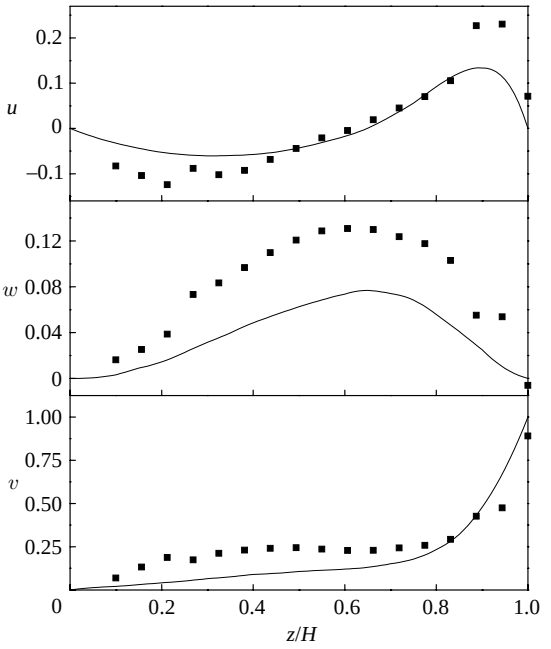

FIGURE 6. Measured velocity profile of the non-dimensional components $u = v_r/\Omega r$, $w = v_z/\Omega r$ and $v = v_\varphi/\Omega r$ at $r = 1.0$ cm for $Re_2 = 104$. The lines are the corresponding components for infinite disks extrapolated from Joseph's numerical solution. The error bars are of the same order as the symbols' dimension.

beyond $r = 0.2L$, which is the radial distance where we performed the measurements. As figure 5 shows, for Re_1 our experimental data are surprisingly consistent with Joseph's data.

On the other hand, at $Re > Re_C$, Brady & Durlofsky found that the flow for a closed end only qualitatively resembled Batchelor solution, consisting of two separated boundary layers close to the disks and a core rotating as a solid body. This is just what our data (figure 6) show for $Re = Re_2$: the azimuthal velocity follows that behaviour, while there is no longer consistency between the experimental data and the similarity solution interpolated for $Re = 104$ from Joseph's data.

In conclusion, we have implemented an heterodyne light scattering setup in order to measure the velocity field of swirling flow with a fixed and a rotating disk for a closed end condition. For two different Reynolds number, we measured the three components of the velocity field by making a scan along the gap, in the vicinity of the axis of rotation. Brady & Durlofsky studied the swirling flow for finite disks and found that the solution is of the similarity form for $Re < Re_C$ in a region near the axis, which gets smaller as Re increases. Our results for $Re_1 < Re_C$, performed in the vicinity of the axis, are in very good agreement with a numerical solution of the similarity equations. Besides, Brady & Durlofsky found that, for $Re > Re_C$, there is no longer agreement between the finite and infinite disk solution anywhere in the flow domain, but the closed-end flow resembles qualitatively the Batchelor solution near the axis. Again, our results for $Re_2 > Re_C$ validate the theoretical predictions, as the azimuthal velocity shows a core rotating as a solid body and two boundary layers, which is the typical behaviour described by the Batchelor solution, while there is no

longer agreement between our data and a numerical solution of the corresponding similarity equations.

We wish to thank F. Zamponi for having designed the cell used in the experiment and for useful discussions; we also thank G. Bolle, M. Pallagrossi, C. Piacenti, A. Salvati and Md Islam Deen for technical assistance.

REFERENCES

Batchelor, G. K. 1951 Note on a class of solutions of the Navier–Stokes equations representing steady rotationally-symmetric flow. *Q. J. Mech. Appl. Maths* **4**, 29–41.

Berne, B. J. & Pecora, R. 1976 *Dynamic Light Scattering*. Dover.

Bien, F. & Penner, S. S. 1969 Velocity profiles in a steady and unsteady rotating flows for a finite cylindrical geometry. *Phys. Fluids* **13**, 1665–1671.

Brady, J. F. & Durlofsky, L. 1987 On rotating disk flow. *J. Fluid Mech.* **175**, 363–394.

Cummins, H. Z. & Swinney, H. L. 1970 Light beating spectroscopy and Light scattering theory. *Progress in Optics*, vol. VIII (ed. E. Wolf). Elsevier North-Holland.

Dijkstra, D. & van Heijst, G. J. F. 1982 The flow between two finite rotating disks enclosed by a cilinder. *J. Fluid Mech.* **128**, 123–154.

Drain, L. E. 1980 *The Laser Doppler Technique*. Wiley & Sons.

Fuller, G. G., Rallison, J. M., Schmidt, R. L. & Leal, L. G. 1980 The measurements of velocity gradients in laminar flow by homodyne light-scattering spectroscopy. *J. Fluid Mech.* **100**, 555–575.

Hewitt, R. E. & Duck, P. W. 1999 Non-axisymmetric rotating-disk flows: nonlinear travelling-wave states. *J. Fluid Mech.* **413**, 287–316.

Johnson, C. S. & Gabriel, D. A. Jr. 1994 *Laser Light Scattering*. Dover.

Joseph, D. D. 1990 *Fluid Dynamics of Viscoelastic Liquids*. Springer.

Kármán, T. von 1921 Laminar und turbolente reibung. *Z. Angew. Math. Mech.* **1**, 233–252.

Larson, R. G. 1998 *The Structure and Rheology of Complex Fluids*. Oxford University Press.

Prasad, A. K. & Adrian, R. J. 1992 Stereoscopic particle image velocimetry applied to liquid flows. *Exps. Fluids* **15**, 49–60.

Ricka, J. 1993 Dynamic light scattering with single-mode and multimode receivers. *Appl. Opt.* **32**, 2860–2875.

Salmon, J.-B., Manneville, S., Colin, A. & Pouligny, B. 2003 An optical fibre based interferometer to measure velocity profiles in sheared complex fluids. *Eur. Phys. J. AP* **22**, 143–155.

Stewartson, K. 1953 On the flow between rotating coaxial disks. *Proc. Camb. Phil. Soc.* **49**, 333–341.

Tong, P., Goldburg, W. I. & Chan, C. K. 1988 Turbolent transition by photon-correlation spectroscopy. *Phys. Rev.* A **37**, 2125–2133.

Zandbergen, P. J. & Dijkstra, D. 1987 von Kármán swirling flows. *Annu. Rev. Fluid Mech.* **19**, 465–491.